quantum beam science

MDPI

Article

Laser-Induced Breakdown Spectroscopy and X-ray Fluorescence Analysis of Bronze Objects from the Late Bronze Age Baley Settlement, Bulgaria

Petya Penkova [1], Galina Malcheva [2], Margarita Grozeva [2], Tanya Hristova [1], Georgy Ivanov [1], Stefan Alexandrov [1], Kiril Blagoev [2], Vani Tankova [2] and Valentin Mihailov [2,*]

[1] National Archaeological Institute with Museum, Bulgarian Academy of Sciences, 2 Saborna Str., 1000 Sofia, Bulgaria
[2] Institute of Solid State Physics, Bulgarian Academy of Sciences, 72 Tzarigradsko Chaussee, 1784 Sofia, Bulgaria
* Correspondence: valentin@issp.bas.bg

Abstract: In the presented work, a total of 60 bronze artefacts from the prehistoric settlement of Baley, Bulgaria were analyzed by means of laser-induced breakdown spectroscopy (LIBS) and X-ray fluorescence spectroscopy (XRF). The archaeological finds were excavated from three levels, with a time span from the 15th century BC to the first half of the 11th century BC. The obtained analytical information was used for quantitative estimation of the amount of tin, lead and arsenic, which determine the mechanical properties of the alloy and the manufacturing technology. Based on the estimated quantities of these elements, a chemometric statistical analysis (principal component analysis—PCA) was performed to classify and divide the samples into separate groups according to the production dating. The data obtained in this study can be used for comparison with the elemental content in deposits from other settlements of this period.

Keywords: LIBS; XRF; principal component analysis; archaeometry

Citation: Penkova, P.; Malcheva, G.; Grozeva, M.; Hristova, T.; Ivanov, G.; Alexandrov, S.; Blagoev, K.; Tankova, V.; Mihailov, V. Laser-Induced Breakdown Spectroscopy and X-ray Fluorescence Analysis of Bronze Objects from the Late Bronze Age Baley Settlement, Bulgaria. *Quantum Beam Sci.* **2023**, *7*, 22. https://doi.org/10.3390/qubs7030022

Academic Editor: Hiroyuki Aoki

Received: 28 April 2023
Revised: 7 June 2023
Accepted: 28 June 2023
Published: 13 July 2023

1. Introduction

The Bronze Age is a historical period lasting approximately from 3300 BC to 1200 BC and varying even within the European continent. This is due to the use of relatively scarce deposits of copper and especially tin, which suggests the presence of a developed trade network. In addition, specific manufacturing techniques are required to produce a bronze alloy. For this purpose, interaction and exchange of knowledge between individual cultures are also necessary.

New metal alloys with different compositions, properties and functions appeared during the Bronze Age and technologies for their production were developed. The main elements added to copper to make bronze are arsenic and tin, although they are rarely used together. Lead can also be considered as a secondary additive, and it can sometimes be a major component of bronze. For example, arsenic content was relatively high during the Early Bronze Age, and this element was replaced first by tin during the Middle Bronze Age, by tin–lead alloys during the Late Bronze Age, and finally by iron during the Iron Age. The concentration of alloying elements in bronze significantly affects its characteristics, such as the melting temperature and ductility. Forging processes (hot or cold) are directly related to ductility, while the melting temperature is related to the casting process [1]. In addition, the presence of some elements as additives with different concentrations in the alloy gives information about the change of technologies over time. Therefore, the knowledge of the quantitative composition of the elements in the alloy can provide information about the production technology of the artifacts, possibility dating and classification of objects according to their function [2].

A chronological classification of the Bronze Age, based on the elemental composition of the bronze used to make objects in the Oriental Mediterranean, covers the period from 3500 BC to 1150/1050 BC. It can be divided into three distinct periods: the Early Bronze Age (3500–2000 BC), Middle Bronze Age (2000–1600 BC) and Late Bronze Age (1600–1150/1050 BC). The contents of Cu, Sn, Pb and As vary during the indicated periods, the most commonly found concentrations being the following: the Early Bronze Age (Cu (80%), Sn (0.1%), As (2%)), Middle Bronze Age (Cu (80%), Sn (6%), Pb (0.1%), As (0.5%)) and Late Bronze Age (Cu (80%), Sn (12%), Pb (2%), As (0.2%)) [3]. It should be noted, however, that the different periods overlap because new techniques appear while the previous ones continue to develop and improve.

Today, the main methods for studying the elemental composition of archaeological sites are X-ray photoemission spectroscopy (XPS) [4], atomic absorption spectroscopy (AAS) [5], scanning electron microscopy (SEM) [6,7] and inductively coupled plasma–mass spectrometry (ICP-MS) [8,9]. For a molecular analysis, commonly used methods are Raman spectroscopy [10,11] and Fourier transform infrared spectroscopy (FTIR) [12,13]. Some of these techniques are destructive and not suitable for archaeological objects that are valuable, while others require an analysis of the objects in a laboratory, which is not always possible. In general, these methods are complex, expensive and unable to handle large sample sizes.

Over the past 20 years, LIBS and XRF have been established as validating and complementary techniques for the study of archaeological finds. Recently, the integrated use of both methods has been successfully applied for the investigation of calcareous and refractory building materials [14], copper alloys [15–21], archaeological pottery [22], silver coins [23], comparative studies of pigments and paints, glazed ceramics and Roman coins [24].

In the LIBS method, a very small volume from the surface layer is used, and the XRF is non-destructive. Both methods are convenient for providing an elemental composition analysis of ancient artefacts. This makes them very useful to both restorers and archaeologists, yielding important information about the production technology and the clarification of the nature of the destructive processes of the artifacts. Although the analytical characteristics such as accuracy and reproducibility of LIBS analyses are not quite satisfactory, they are compensated by other characteristics such as rapidity and the possibility of an on-site analysis, which makes LIBS a suitable method for a micro-destructive quantitative analysis. Other advantages of LIBS are the high spatial resolution and the ability to measure the depth distribution profile of the elements in the sample with successive laser pulses at the same point. Laser-induced breakdown spectroscopy is a widely used tool for characterization in the field of cultural and historical heritage. Archaeological samples examined include metals, ceramics and glass [25–28]. The application of the LIBS method both in archaeology and industry is a subject of a number of books [29–31] and review articles [32–34].

The aim of our research was to determine the concentration of the main elements arsenic, tin and lead in bronze objects excavated from three successive levels from collective deposition at the Baley settlement, Bulgaria. This settlement is the largest one coming from a well-established stratigraphic complex from the second millennium BC Lower Danube. Based on the obtained data, a principal component analysis (PCA) is applied in order to find out if the objects from individual levels differ from each other according to the contents of alloying elements—Sn, Pb and As—and thus to compare the bronze alloy in different periods. Based on this information, assumptions about the improvement in production technology over the years could be made. There is a variety of analytical studies which are combined with PCA [35–37].

2. Prehistoric Complex Baley

The prehistoric complex Baley, representing a settlement and necropolis, is located in North-West Bulgaria, on a non-flooded sand dune at the right bank of the Timok River, approximately 2 km south of its confluence with the Danube River (Figure 1). With its

secure stratigraphic position and variety of metal types, the Baley lot provides a good opportunity to enlighten upon Late Bronze Age production and distribution of bronze objects in the Lower and Middle Danube regions and Transylvania. It could also provide additional data on the largely discussed problems related to trade routes and exchange in Central and Southeastern Europe during the second half of the second millennium BC.

Figure 1. Map of Balkan peninsula with Baley settlement location (●).

Four main occupation Late Bronze Age levels have been established in the settlement, described as "building horizons" and detected at 0–0.10 m in-depth (level I); 0.40–0.50 m in-depth (level II); 0.80–0.90 m in-depth (level III); and 1.30–1.40 m in-depth (level IV) (Figure 2).

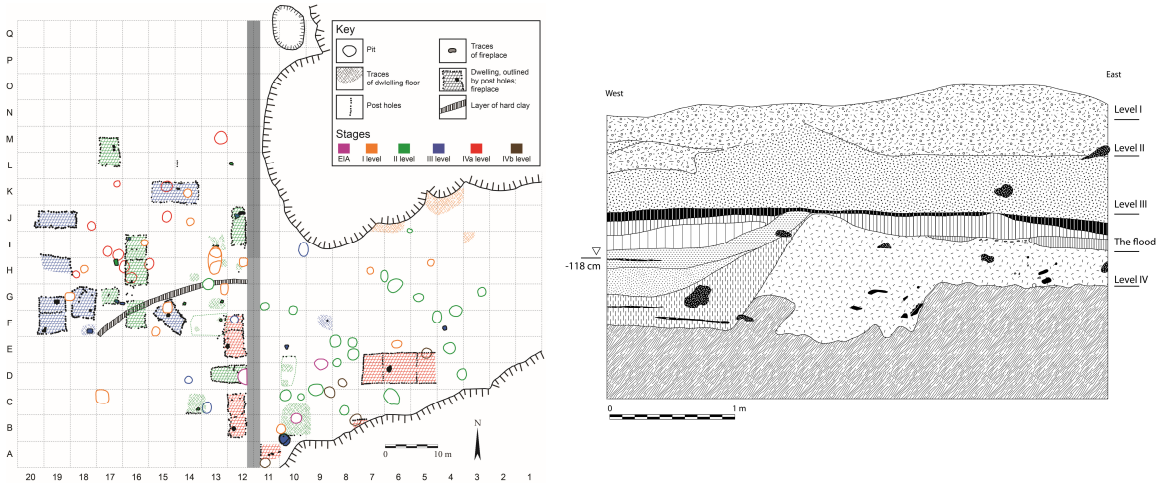

Figure 2. Horizontal plan of the features investigated according to the building levels and profile in box-grid G10 with the four building levels.

Based on the radiocarbon dating of both the settlement and the necropolis, the following chronological sequence of the Baley settlement was established: levels IVb and IVa date to the 15th century BC; levels III-II date to the 14th–first half of the 13th century BC; and level I dates to the second half of the 13th–first half of the 11th century BC. The archaeological complex's investigation and stratigraphy and radiocarbon dating made the Baley site one of the key Lower Danube complexes to improve our knowledge about the historical development during the second half of the second millennium BC in the region, the transition to the Early Iron Age period there and the processes related to the emergence at the historical scene of the ancient Paleo-Balkanic tribes [38].

3. Materials and Methods

3.1. Investigated Artefacts

The settlement's bronze object collection includes weapons, tools, hair rings, pins and jewelry as follows: Level I a/b—2; Level II—30; Level III—23; Level IVa/b—7; and stray finds from the settlement area—2. The number of bronze objects discovered in the necropolis until 2021 is smaller: one applique and two hair rings from the Middle Bronze Age graves; one applique, one knife, one bracelet, one needle and two small fragments from the Late Bronze Age graves. Examples of objects are presented in Figure 3.

Figure 3. Examples of Baley settlement bronze objects: (**a**) dagger handle (sample 237); (**b**) pendant (sample 396); (**c**) hair ring (sample 279); (**d**) decoration (sample 782).

The imbalance between the findings from the settlement and the necropolis, as well as the fact that the excavations of the necropolis are still ongoing, determined our decision to focus on the analysis of the settlement's lot only. The two objects found on the first level and the stray finds were also not included in this study.

3.2. Methods

Two methods for an elemental analysis of the artefact composition were applied, laser-induced breakdown spectroscopy (LIBS) and X-ray fluorescence (XRF). The micro-destructive nature of LIBS and the non-destructive nature of XRF are convenient for providing an elemental composition analysis of ancient artefacts.

In the present work, LIBS and XRF are used as complementary methods, where XRF serves as a validating technique for the LIBS analysis. Both techniques have their advantages and disadvantages. The LIBS technique can detect all elements, while the XRF tech-

nique is applied for the determination of elements with an atomic number Z > 11 [39–41]. On the other hand, in conventional XRF, the analytical signal is collected from a larger area than in LIBS, and thus errors due to sample inhomogeneities are minimized. The typical spot size at the sample surface in XRF measurements ranges in diameter from several hundred micrometers up to several millimeters, and in the LIBS measurements, the spot size varies from several tens of micrometers up to several hundred micrometers. The drawback of XRF is that it provides analytical information only on the surface, while the LIBS technique has the ability to analyze the material in depth, without the need of object fragmentation. A disadvantage of LIBS is its relatively low signal to noise ratio. Also, LIBS has a low signal reproducibility due to fluctuations in the laser fluence and focus and its sensitivity to material inhomogeneity, making it less appropriate for a quantitative analysis than XRF. Due to the comparatively low sensitivity of LIBS to arsenic and the limited number of arsenic spectral lines, XRF complements LIBS in the quantification of arsenic.

3.2.1. Laser-Induced Breakdown Spectroscopy

A standard LIBS setup based on a nanosecond Q-switched Nd:YAG laser (Quanta Ray GCR3) operating at the fundamental wavelength of 1064 nm (pulse duration, 8 ns; laser pulse energy, 10 mJ; repetition rate, 1 Hz) was used. The laser beam was focused with a lens (f = 170 mm) at 1 mm behind the surface of the sample, creating a plasma plume. The laser spot size was approximately 300 μm in diameter and the laser fluence was about 44 J/cm^2. The light emitted from the plume was collected by an optical fiber (50 μm in diameter) and analyzed with an Eschelle-type spectrometer (Mechelle 5000) using 52 lines/mm grating with a spectral resolution of 0.04 nm at 250 nm or 0.1 nm at 800 nm. The spectra were recorded with an intensified charge-coupled device (ICCD) camera (DH734-18F-03, Andor Technology) with 1024 × 1024 pixels. The detector was gated with a delay/pulse generator type G5-56. To discriminate the atomic and ionic emission from the continuum background of the plasma emission, a delay time of 1 μs and a gate of 1 μs were used. The analyses were performed registering a kinetic series of 15 successive spectra each, with 10 accumulated spectra measured at one spot. The spectrometer was calibrated with deuterium and Hg/Ar standard lamps for the intensity and wavelength, respectively, in the 220–850 nm spectral range. The experimental parameters were optimized to obtain a good signal-to-noise ratio and to assure the best measurement reproducibility.

3.2.2. X-ray Fluorescence Spectroscopy

The instrument used was an ED-XRF spectrometer EDX–720 (Shimadzu, Kyoto, Japan). The measurement conditions were as follows: atmosphere—air; collimator—1 mm; 50 kV for 100 s. The elements in the samples were identified based on the characteristic X-ray lines in the energy range 0–40 keV. Since non-destructivity is one of the main requirements for analyzing museum objects, the instrument chamber was rather big, 30 cm in diameter and 15 cm in height, which allows for placing objects inside without the necessity of sampling.

3.2.3. Principal Component Analysis

In order to trace a possible technology development of production of the bronze objects, a chemometric method (principal component analysis—PCA) was used. PCA is a statistical technique utilized to find the correlations between a multitude of variables and thus to cluster the investigated samples according to their material differences and resemblances. The essence of this method lies in the reduction in the dimensionality of the multivariate data set. This is accomplished by compression of the original data set to a newly established smaller number of uncorrelated variables, while preserving the maximum of the information contained in the initial data. These new variables are linear combinations of the original variables and are known as principal components (PCs) [42,43]. A detailed explanation of the fundamentals and the mathematical background of PCA can be found in the literature [44].

4. Results and Discussion

In the present work, a quantitative analysis was carried out to determine the concentration of tin, lead and arsenic in a total of 60 bronze objects examined. The concentration of tin and lead was measured with LIBS, and the concentration of arsenic was measured with XRF.

When analyzing metal artefacts, it is very important to take into account several factors that might affect the reliability of the qualitative and quantitative results. The elemental composition of the original alloy is usually affected by corrosion, which can cause a change in the weight ratio of certain elements.

A second factor is the heterogeneous character of the alloy used for object production, which can be a result of poor mixing of the components, cooling, etc., in the process of manufacturing. To avoid these effects, the surface analytical techniques (XRF) require preliminary sample preparation—a small part of the surface of the objects is mechanically cleaned from the corrosion layer, and then the analyses are performed. When using a LIBS analysis, this is not necessary because the laser pulses can be used for this purpose. Since LIBS analyses are performed on surfaces uncleaned of corrosion products, kinetic series of 15 successive spectra each, with 10 accumulated spectra, are measured at one spot.

The corroded surface of Cu-Sn alloys (the so-called patina) consists mostly of copper salts and, in rare cases, a considerable concentration of tin [45]. Figure 4 demonstrates a part of the spectrum in the range 324–328 nm for one of the investigated samples (where the increased amount of these elements on the surface layer can be seen), with the spectral lines of Cu and Sn. The first three to five spectra correspond to the patina, and the following spectra exhibit a relatively constant intensity of the lines. The patina spectra were excluded from the LIBS analysis.

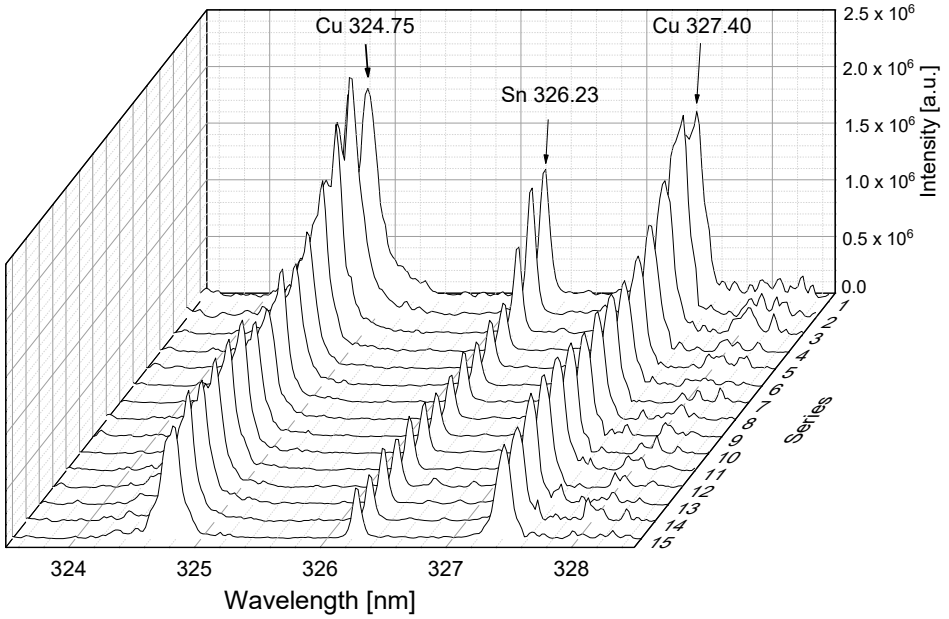

Figure 4. Part of the kinetic series for one of the investigated samples, demonstrating in-depth intensity alteration of Cu and Sn spectral lines.

For qualitative determination of tin and lead with LIBS, the following spectral lines were used: Pb I, 283.31 nm; Pb I, 368.35 nm; Pb I, 405.78 nm; Sn I, 284.00 nm; Sn I, 286.33 nm; Sn I, 300.91 nm; Sn I, 317.50 nm; and Sn I, 326.23 nm. All spectroscopic data used for the LIBS recorded spectral lines are provided by NIST [46]. A representative spectrum obtained from the LIBS analysis for one of the investigated samples for the spectral region 220–850 nm is shown in Figure 5.

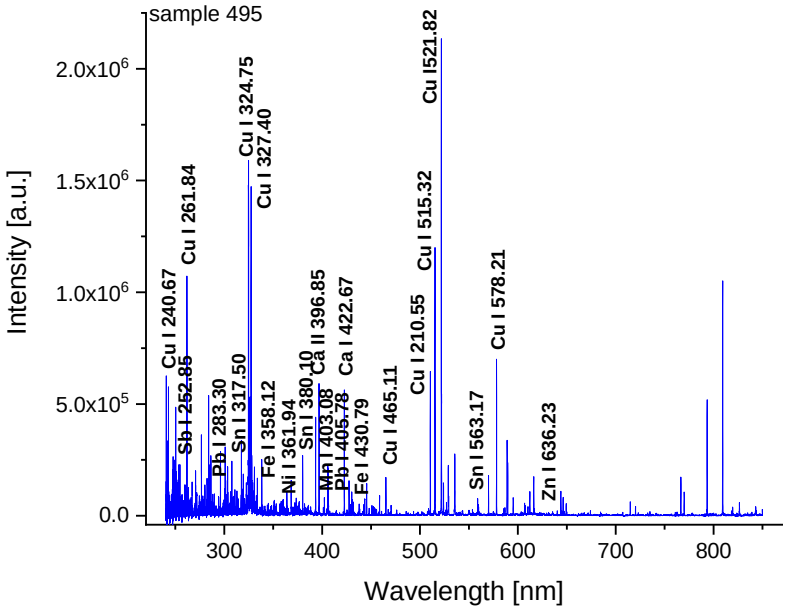

Figure 5. Representative spectrum obtained for one of the investigated samples.

Figure 6 presents exemplary LIBS spectra with some of the spectral lines of Cu, Pb and Sn in two spectral regions (280–290 nm and 320–330 nm) obtained for three of the investigated objects with different amounts of Sn and Pb (samples 285, 396 and 779).

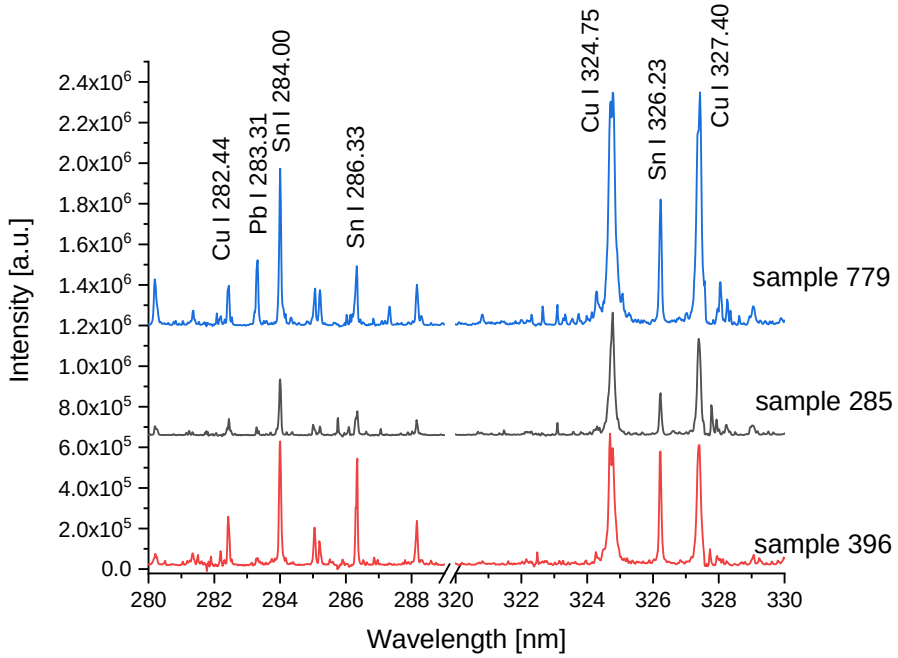

Figure 6. Exemplary LIBS spectra representing some of the spectral lines of Cu, Pb and Sn obtained for three of the investigated objects (samples 285, 396 and 779).

The elements of interest in XRF analyses were detected with the characteristic emission lines: Sn ($K\alpha_1$ at 25.27 keV, $K\alpha_2$ at 25.04 keV, $K\beta$ at 28.49 keV, $L\alpha_1$ at 3.44 keV), Pb ($L\alpha_1$ at 10.55 keV, $L\beta_1$ at 12.61 keV, $L\gamma$ at 14.76 keV) and As ($K\beta$ at 11.73 keV). Figure 7 presents exemplary XRF spectra for two of the investigated objects.

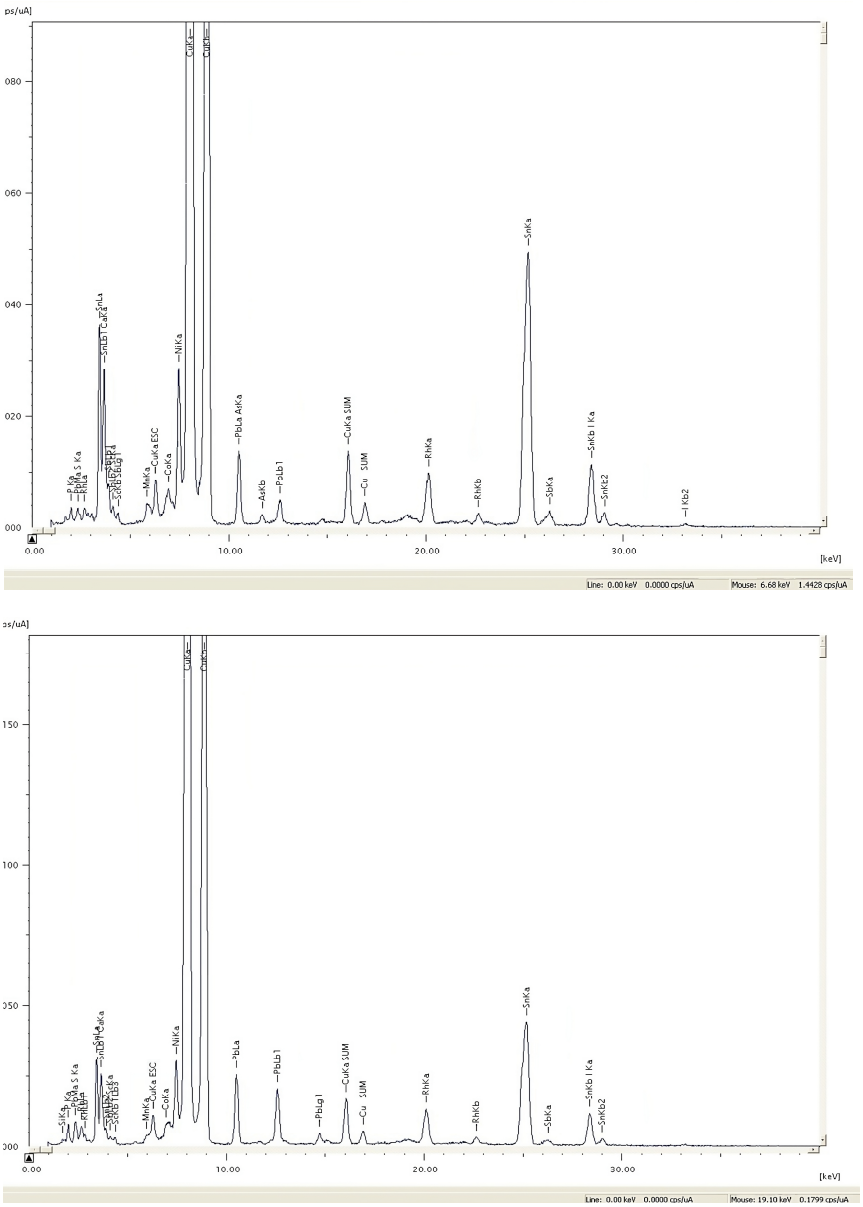

Figure 7. XRF spectra registered for two of the samples—285 and 779.

For the quantification of the LIBS data, the standard reference materials 42.23-2, 50.01-4, 50.04-4 and 71.32-4 were used, produced by the Bureau of Analysed Samples LTD (BAS), Middlesbrough, UK (Catalogue No. 852, 2017). Calibration curves were constructed by plotting the normalized intensities of selected analytical lines as a function of the analyte concentration in the alloy (Figure 8). Additionally, to minimize fluctuations due to laser instability and matrix effects, the analyte emission was normalized to the emission of copper, which is the main element of the alloy. The calibration curve for determining lead concentrations was constructed by measuring the intensity of the Pb 405.8 nm spectral line normalized to the intensity of the 406.3 nm Cu line used as an internal standard. For the tin calibration curve, the Sn 284.0 nm and Cu 282.4 nm lines were used. These analytical spectral lines were selected for ratio calculations because they do not overlap and do not suffer self-absorption effects. The values for the standard deviation of the mean were in the range of 10–20%.

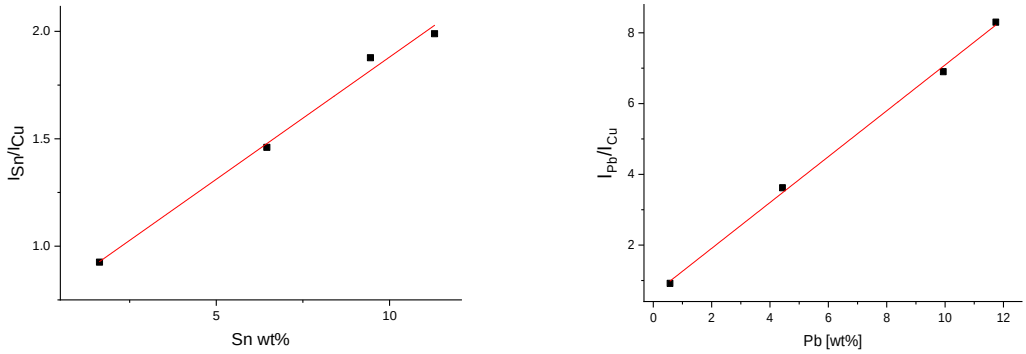

Figure 8. Calibration curves for tin and lead.

Altogether, 60 bronze objects were investigated and the results are presented in Table 1. As expected for Late Bronze Age objects, all samples contain tin as a major element. Lead was also found in all samples, which is one of the elements determining the mechanical properties of the alloy. Arsenic, also a technologically important element for the Bronze Age, was found in most of the objects. From the results of the analyzed objects, it can be assumed that the Late Bronze Age bronzes from Baley are highly variable in composition.

Table 1. Tin, lead and arsenic concentration of the analyzed objects (in wt%).

Level	Sample No.	Sn (LIBS)	Sn (XRF)	Pb (LIBS)	Pb (XRF)	As (XRF)	Sample Description
II	100	9.3	9.51	0.39	0.3	0.48	Decorative needle
	160	n.m.	11.43	n.m.	0.51	0.23	Hair ring
	172	10.6	12.49	0.6	0.72	0.48	Decorative needle
	174	5.82	6.31	0.25	0.37	0.64	Awl
	180	9.0	8.9	0.3	0.31	0.52	Awl fragment
	213	8.83	10.1	0.34	0.47	0.45	Decorative needle
	214	n.m.	12.27	n.m.	0.26	n.d.	Decorative needle
	237	14.2	15.05	0.46	0.63	0.36	Dagger handle
	238	8.0	8.49	0.7	0.88	0.91	Decoration
	264	14.6	14.68	0.25	0.4	1.02	Decorative needle
	268	8.0	9.72	0.3	0.82	0.69	Decorative needle
	269	21.2	26.35	1.4	1.01	0.31	Pendant
	270	8.9	8.43	0.19	0.25	0.37	Decorative needle
	273	21.4	18.42	0.7	0.96	0.36	Decorative needle
	280	12.4	14.32	0.2	0.27	0.27	Pendant
	285	5.11	6.38	0.23	0.39	0.55	Knife edge
	287	n.m.	10.21	n.m.	n.d.	n.d.	Saltaleone
	290	10.5	11.59	0.27	0.21	0.36	Decorative needle
	302	13.2	13.22	0.5	0.48	0.40	Sewing needle
	303	19.0	14.53	0.1	n.d.	0.25	Decorative needle
	305	8.0	9.02	0.19	0.18	0.43	Knife edge
	357	12.0	9.46	0.35	0.22	0.52	Axe
	495	n.m.	4.16	n.m.	0.67	1.92	Decoration
	501	11.9	13.8	0.1	n.d.	0.35	Decorative needle
	503	9.0	11.08	0.2	0.34	n.d.	Decoration
	520	13.1	16.0	0.11	0.7	0.57	Decoration
	559	10.0	12.4	0.12	n.d.	1.41	Hook

Table 1. *Cont.*

Level	Sample No.	Sn (LIBS)	Sn (XRF)	Pb (LIBS)	Pb (XRF)	As (XRF)	Sample Description
III	101	8.5	10.69	0.5	0.64	0.51	Decorative needle
	108	7.3	6.01	0.41	0.48	n.d.	Decorative needle
	115	16.8	16.30	0.3	0.26	0.43	Awl
	274	8.0	9.16	0.3	0.52	0.56	Awl
	281	19.2	22.81	0.4	0.54	0.33	Pendant
	282	12.1	10.64	0.2	0.27	0.42	Sewing needle
	284	12.7	13.79	1.4	1.44	0.21	Decorative needle
	p284	12.6	11.5	0.5	1.55	0.22	Decorative needle
	300	10.3	12.22	0.3	0.45	0.48	Decorative needle
	301	11.7	12.86	1.25	1.30	0.39	Decorative needle
	304	8.1	10.80	0.52	0.68	0.31	Sewing needle
	306	21.7	18.45	0.41	0.43	0.28	Decoration
	308	13.4	10.24	0.13	0.19	0.22	Knife edge
	318	17.8	16.56	3.0	2.32	0.63	Axe
	342	13.2	14.17	0.5	0.3	0.46	Decorative needle
	343	n.m.	16.95	n.m.	0.48	0.41	Decorative needle
	396	25.8	25.06	0.63	0.68	0.61	Pendant
	404	8.2	11.5	0.17	n.d.	0.83	Decorative needle
	409	14.0	26.58	0.2	0.4	0.65	Decorative needle
	410	11.6	12.19	0.21	0.3	0.43	Awl
	452	17.0	19.5	2.3	1.5	0.71	Decoration
	463	7.9	12.83	0.2	0.42	2.27	Awl
	778	10.6	13.53	0.1	n.d.	0.81	Hook
	779	10.8	9.8	3.6	3.3	0.2	Sewing needle
IV	278	20.8	18.49	0.1	n.d.	0.48	Hair ring
	279	12.2	15.59	0.51	0.67	0.49	Hair ring
	309	15.1	16.41	0.28	0.32	0.7	Hair ring
	487	n.m.	12.36	n.m.	0.23	0.24	Indefinable object
	729	n.m.	14.08	n.m.	0.24	0.45	Sewing needle
	748	7.8	10.5	0.1	n.d.	0.61	Razor
	782	12.05	12.6	0.77	0.85	0.43	Decoration

n.d.—not detected; n.m.—not measured.

The tin concentration in the majority of the investigated objects varies between 8 wt% and 18 wt%, except for four samples, which are with a tin concentration over 20 wt% (sample 269—26.35%, sample 281—22.81%, sample 396—25.06% and sample 409—26.58%). It is known that tin is added to copper to make it harder [47].

Usually, a bronze alloy with about 8% tin is hard and, at the same time, plastic enough to be easily processed. When the tin content exceeds 8%, the alloy becomes harder and requires repeated annealing to be cold-worked. It is considered that the optimal value of the tin concentration is in the range of 8–12%. Bronze with high tin content (over 12%) is only suitable for hot processing because the higher tin content makes the alloy too hard and brittle, which leads to cracking when cold-working is attempted. It is also stated that a tin concentration above 15% changes the color of bronze from reddish to golden [48]. Taking into account that the four exceptions are decorations (samples 269, 281 and 396 are pendants and sample 409 is a decorative needle), it can be assumed that the higher tin content was probably added to achieve certain coloration.

As a whole, the lead concentration in most of the objects is below 1% (approximately 0.1% to 0.9%) with only six exceptions being up to 3.3% (sample 284—1.44%, sample p284—1.5%, sample 301—1.3%, sample 318—2.32%, sample 452—1.5% and sample 779—3.3%). A lead content over 1–2% is considered to have been added purposefully [49]. Five of the six exception objects are with a lead content between 1% and 2%, so it is not clear whether it was added intentionally or if it is an impurity. One of the objects, sample 779, has 3.3% lead, which suggests that lead may have been added as an alloying element. Basically, lead is added to bronze in order to lower the melting point of the alloy and to

make it more castable. Bronzes with added lead are not suitable for cold-working like hammering [50].

The arsenic concentration in almost all of the samples was lower than 1%, with an exception of four objects having an arsenic concentration in the range of 1.4–2.3% (sample 559—1.41%, sample 495—1.92% and sample 463—2.27%). It is accepted that a concentration of arsenic below 1% can be attributed to its presence in the copper ore [51], while copper alloys containing more than 1% arsenic would be intentional products [52]. In prehistory, arsenic bronzes contain from 2% to more than 8% arsenic and it is usually used at a content of about 3 wt%, since higher contents do not significantly improve its hardness. Arsenic copper elements can be both hammered and forged essentially without cracking and make the alloy especially suitable for casting. Concentrations between 2% and 3% may also lighten the color of the alloy. Since arsenic copper is typical for the Early Bronze Age, it can be suggested that the sample with the highest As content (sample 463) is recycled from older objects.

In an attempt to find the possible distinction of the samples excavated from different levels according to tin, lead and arsenic concentrations, the data were statistically processed by means of the PCA technique. This method is convenient for extracting information that is not easily observed from a multiple data set. In this work, Origin Pro 2018 software was employed for the PCA analysis. The result is shown on the biplot of the first two principal components, PC1 and PC2. A biplot represents the loading plot and score plot in one graph. The score plot shows the pattern of samples based on their similarities and differences and the loading plot reveals how strongly each variable influences the PCs. The first two PCs account for 72.24% of the cumulative variance. PC1 explains 42.08% of the variation and PC2 explains 30.16%. In Figure 9, it is seen that PC1 has strong negative loading for As and positive loading for Sn and Pb, while PC2 has positive loading for Pb and negative loading for Sn.

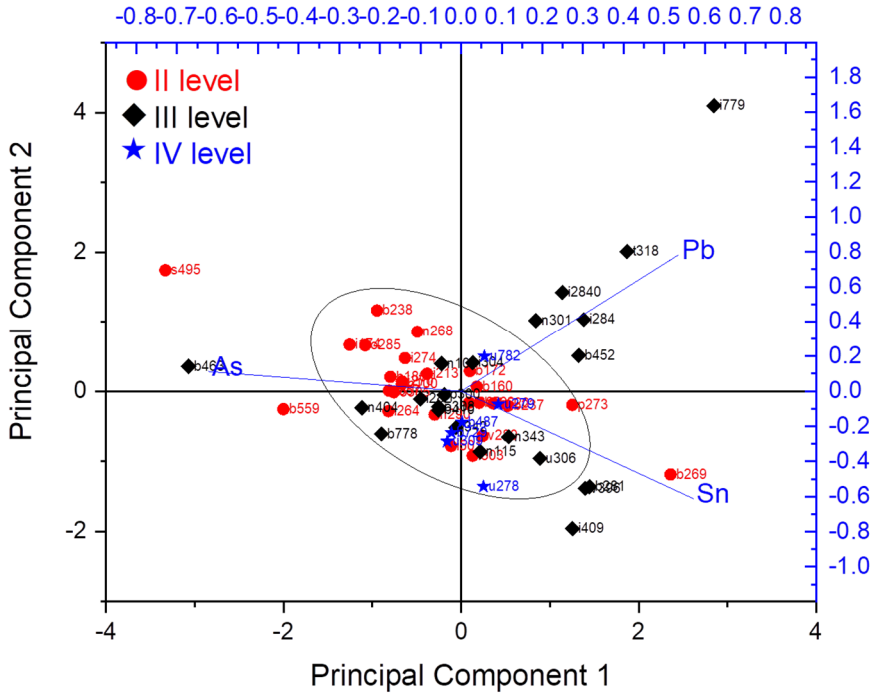

Figure 9. PCA biplot from the sample measurement data for all of the investigated objects.

The score plot shows that part of the samples from the II and III levels (red and black dots, respectively) and all of the samples from the IV level (blue dots) overlap at the center of the graph. Still, a separation between the artifacts from the II level and III level can be seen, influenced mainly by tin and to some extent by lead. Most of the samples from the III and IV levels are located at the positive part of PC1, while many of the samples from the II

level are at the negative part of PC1. It can also be noticed that the samples from the II and IV levels are more clustered than the ones from the III level, which are more spread.

The narrowing of the range of tin content closer to optimal values in the samples from the II level could be attributed to the optimization of the production technology of a bronze alloy. Another possible explanation is a narrowing of the range of raw material sources.

All exceptions from the ranges of Sn, Pb and As (Sn: 8–18%, Pb: 0.1–0.9% and As < 1%) obtained with LIBS and XRF analyses are visualized on the PCA graph. The four exceptions with tin over 20% are seen in the PCA graph as outlier scores separated from the others on the positive part of PC1 and the negative part of PC2. The six samples with lead over 1% are located at the positive parts of PC1 and PC2. The three exceptions with higher arsenic content are characterized by the highest negative scores on PC1.

5. Conclusions

In this study, elemental analyses are presented of bronze objects from the Baley settlement, the biggest one from the second millennium BC in the Lower Danube area, especially in its western part.

The results from quantitative elemental analyses for tin, lead and arsenic show that the examined objects are made of tin bronze, whose content falls within the ranges characteristic of the Late Bronze Age. There are several exceptions with very high tin concentrations. All of them are decorations and jewelry, which may suggest that high tin content was used for obtaining certain coloration. The arsenic content is minimal (except for one item), suggesting that it stems from the ore and was not intentionally added.

The PCA analyses allow objects to be grouped according to horizons, which cannot be conducted directly from the elemental concentration results. The clustering of samples from the II level compared to samples from the III level is indicative of the process of optimizing tin and lead content, as well as possible different sources of raw material. To specify the manufacturing technologies of the various-object production, additional structural analyses are needed, which will be the task of an upcoming study.

The analyses presented here are in fact the first attempt to explore the Late Bronze Age bronze artefact production in this region on such a scale. In our opinion, the data presented here could and should be regarded as a first step towards a better and much more elaborated investigation of the problems related to the "chaîne opératoire" of bronze production and distribution in the western part of the Lower Danube during the second half of the second millennium BC. The data presented here can be used in the future for comparison with the elemental content in deposits from other settlements of this period.

Author Contributions: Conceptualization, P.P., S.A., V.M. and K.B.; methodology, V.M. and T.H.; formal analysis, V.M. and V.T.; validation, S.A., G.I. and T.H.; archaeological investigation, T.H., S.A. and G.I.; resources, G.I.; experimental data, P.P., G.M., M.G., K.B. and V.T.; writing—original draft preparation, T.H. and V.M.; writing—review and editing, M.G., V.M., K.B. and V.T. All authors have read and agreed to the published version of the manuscript.

Funding: This work was partially supported by the Bulgarian Ministry of Education and Science under the National Research Programme "Young scientists and postdoctoral students-2" approved by DCM 206/07.04.2022.

Institutional Review Board Statement: Not applicable.

Informed Consent Statement: Not applicable.

Data Availability Statement: Data is available on request.

Acknowledgments: The authors thank Christina Andrews for proofreading the manuscript.

Conflicts of Interest: The authors declare no conflict of interest.

References

1. Goffer, Z. *Archaeological Chemistry*, 2nd ed.; John Wiley & Sons, Inc.: Hoboken, NJ, USA, 2007; pp. 165–184.
2. Scott, D.; Podany, J.; Considine, B. *Ancient & Historic Metals: Conservation and Scientific Research*; Oxford University Press: Oxford, UK, 1995.
3. Fortes, F.J.; Cortés, M.; Simòn, M.D.; Cabalìn, L.M.; Laserna, J.J. Chronocultural sorting of archaeological bronze objects using laser-induced breakdown spectrometry. *Anal. Chim. Acta* **2005**, *554*, 136–143. [CrossRef]
4. Casaletto, M.P.; Privitera, A.; Figa, V. Nanoscale Investigations of the Corrosion of Metallic Artworks by X-ray Photoemission Spectroscopy. In Proceedings of the 2018 IEEE 4th International Forum on Research and Technology for Society and Industry (RTSI), Palermo, Italy, 10–13 September 2018.
5. Pollard, A.M. (Ed.) Elemental analysis by absorption and emission spectroscopies in the visible and ultraviolet. In *Analytical Chemistry in Archaeology*; Cambridge University Press: Cambridge, UK, 2007; pp. 47–69.
6. Moro, D.; Ulian, G.; Valdre, G. SEM-EDS microanalysis of ultrathin glass and metal fragments: Measurement strategy by Monte Carlo simulation in cultural heritage and archaeology. *Int. J. Conserv. Sci.* **2020**, *11*, 223–232.
7. Ghani-ur-Rahman; Basid, A. Scanning Electron Microscopy in Archaeology: The Analysis of Unknown Specimen Recovered from District Shangla, Pakistan. *J. Asian Civiliz.* **2015**, *38*, 153–164.
8. Vannoorenberghe, M.; Van Acker, T.; Belza, J.; Teetaert, D.; Crombé, P.; Vanhaecke, F. Multi-element LA-ICP-MS analysis of the clay fraction of archaeological pottery in provenance studies: A methodological investigation. *J. Anal. At. Spectrom.* **2020**, *35*, 2686–2696. [CrossRef]
9. Dussubieux, L. LA-ICP-MS analysis of Andean ceramics: Comparability and data correction for datasets acquired over almost two decades. *J. Archaeol. Sci. Rep.* **2023**, *48*, 103856. [CrossRef]
10. Bersani, D.; Conti, C.; Matousek, P.; Pozzi, F.; Vandenabeele, P. Methodological evolutions of Raman spectroscopy in art and archaeology. *Anal. Methods* **2016**, *8*, 8395–8409. [CrossRef]
11. Ropret, P.; Madariaga, J.M. Applications of Raman spectroscopy in art and archaeology. *J. Raman Spectrosc.* **2014**, *45*, 985–992. [CrossRef]
12. Glavcheva, Z.I.; Yancheva, D.Y.; Kancheva, Y.K.; Velcheva, E.A.; Stamboliyska, B.A. Development of FTIR spectra database of reference art and archaeological materials. *Bulg. Chem. Commun.* **2014**, *46*, 164–169.
13. Legan, L.; Leskovar, T.; Črešnar, M.; Cavalli, F.; Innocenti, D.; Ropret, P. Non-invasive reflection FTIR characterization of archaeological burnt bones: Reference database and case studies. *J. Cult. Herit.* **2020**, *41*, 13–26. [CrossRef]
14. Alberghina, M.F.; Barraco, R.; Brai, M.; Schillaci, T.; Tranchina, L. Double Laser LIBS and micro-XRF spectroscopy applied to characterize materials coming from the Greek-Roman theater of Taormina. *Proc. SPIE* **2009**, *7391*, 61–71.
15. Ferretti, M.; Cristoforetti, G.; Cristoforetti, S.; Palleschi, V.; Salvetti, A.; Tognoni, E.; Console, E.; Palaia, P. In situ study of the Porticello Bronzes by portable X-ray fluorescence and laser-induced breakdown spectroscopy. *Spectrochim. Acta Part B* **2007**, *62*, 1512–1518. [CrossRef]
16. Alberghina, M.F.; Barraco, R.; Brai, M.; Schillaci, T.; Tranchina, L. Comparison of LIBS and m-XRF measurements on bronze alloys for monitoring plasma effects. *J. Phys. Conf. Ser.* **2011**, *275*, 012017. [CrossRef]
17. Wallace, S.; Smith, N.; Nerantzis, N. Handheld Methods in Archaeological Research on Large Copper Alloy Assemblages: HH-XRF Against HH-LIBS. *Archaeometry* **2021**, *63*, 343–371. [CrossRef]
18. Arafat, A.; Na'es, M.; Kantarelou, V.; Haddad, N.; Giakoumaki, A.; Argyropoulos, V.; Anglos, D.; Karydas, A.G. Combined in situ micro-XRF, LIBS and SEM-EDS analysis of base metal and corrosion products for Islamic copper alloyed artefacts from Umm Qais museum. *J. Cult. Herit.* **2013**, *14*, 261–269. [CrossRef]
19. Agresti, J.; Osticioli, I.; Guidotti, M.C.; Kardjilov, N.; Siano, S. Non-invasive archaeometallurgical approach to the investigations of bronze figurines using neutron, laser, and X-ray techniques. *Microchem. J.* **2016**, *124*, 765–774. [CrossRef]
20. Zmuda-Trzebiatowska, I.; del Hoyo-Mel'endez, J.; Śliwiński, G. Material composition evaluation of historical Cu alloy aquamanilia by complementary XRF and LIBS measurements. *Eur. Phys. J. Plus* **2019**, *134*, 269. [CrossRef]
21. Siano, S.; Agresti, J. Archaeometallurgical characterisation of Donatello's Florentine copper alloy masterpieces using portable laser-induced plasma spectroscopy and traditional techniques. *Stud. Conserv.* **2015**, *60*, S106–S119. [CrossRef]
22. Kuzmanovic, M.; Stancalie, A.; Milovanovic, D.; Staicu, A.; Damjanovic-Vasilic, L.J.; Rankovic, D.; Savovic, J. Analysis of lead-based archaeological pottery glazes by laser induced breakdown spectroscopy. *Opt. Laser Technol.* **2021**, *134*, 106599. [CrossRef]
23. Pardini, L.; El Hassan, A.; Ferretti, M.; Foresta, A.; Legnaioli, S.; Lorenzetti, G.; Nebbia, E.; Catalli, F.; Harith, M.A.; Diaz Pace, D.; et al. X-ray Fluorescence and Laser-Induced Breakdown Spectroscopy analysis of Roman silver denarii. *Spectrochim. Acta Part B* **2012**, *74–75*, 156–161. [CrossRef]
24. Lazic, V.; Vadrucci, M.; Fantoni, R.; Chiari, M.; Mazzinghi, A.; Gorghinian, A. Applications of Laser Induced Breakdown Spectros-copy (LIBS) for Cultural Heritage: A Comparison with XRF and PIXE Techniques. *Spectrochim. Acta Part B At. Spectrosc.* **2018**, *149*, 1–14. [CrossRef]
25. Abdelhamid, M.; Grassini, S.; Angelini, E.; Ingo, G.M.; Harith, M.A. Depth profiling of coated metallic artifacts adopting laser-induced breakdown spectrometry. *Spectrochim. Acta Part B At. Spectrosc.* **2010**, *65*, 695–701. [CrossRef]

26. Corsi, M.; Cristoforetti, G.; Giuffrida, M.; Hidalgo, M.; Legnaioli, S.; Masotti, L.; Palleschi, V.; Salvetti, A.; Tognoni, E.; Vallebona, C.; et al. Archaeometric Analysis of Ancient Copper Artefacts by Laser-Induced Breakdown Spectroscopy Technique. *Microchim. Acta* **2005**, *152*, 105–111. [CrossRef]
27. He, J.; Liu, Y.; Pan, C.; Du, X. Identifying Ancient Ceramics Using Laser-Induced Breakdown Spectroscopy Combined with a Back Propagation Neural Network. *Appl. Spectrosc.* **2019**, *73*, 1201–1207. [CrossRef]
28. Singh, P.; Mal, E.; Khare, A.; Sharma, S. A study of archaeological pottery of Northeast India using laser induced breakdown spectroscopy (LIBS). *J. Cult. Herit.* **2018**, *33*, 71–82. [CrossRef]
29. Singh, J.P.; Thakur, S.N. *Laser-Induced Breakdown Spectroscopy*, 2nd ed.; Elsevier Science: Amsterdam, The Netherlands, 2020.
30. Cremers, D.A.; Radziemski, L.J. *Handbook of Laser-Induced Breakdown Spectroscopy*, 1st ed.; Wiley & Sons Ltd.: Chichester, UK, 2006.
31. Foster, P.A. *Guide to Laser-Induced Breakdown Spectroscopy*; Nova Science Pub. Inc.: Hauppauge, NY, USA, 2020.
32. Jolivet, L.; Leprince, M.; Moncayo, S.; Sorbier, L.; Lienemann, C.P.; Motto-Ros, V. Review of the recent advances and applications of LIBS-based imaging. *Spectrochim. Acta Part B At. Spectrosc.* **2019**, *151*, 41–53. [CrossRef]
33. Khan, Z.H.; Ullah, M.H.; Rahman, B.; Talukder, A.I.; Wahadoszamen, M.; Abedin, K.M.; Haider, A.F.M.Y. Laser-Induced Breakdown Spectroscopy (LIBS) for Trace Element Detection: A Review. *J. Spectrosc.* **2022**, *2022*, 3887038. [CrossRef]
34. Detalle, V.; Bai, X. The assets of laser-induced breakdown spectroscopy (LIBS) for the future of heritage science. *Spectrochim. Acta Part B At. Spectrosc.* **2022**, *191*, 106407. [CrossRef]
35. Orlic Bachler, M.; Bišcan, M.; Kregar, Z.; Jelovica Badovinac, I.; Dobrinic, J.; Miloševic´, S. Analysis of antique bronze coins by Laser Induced Breakdown Spectroscopy and multivariate analysis. *Spectrochim. Acta Part B* **2016**, *123*, 163–170. [CrossRef]
36. Moncayo, S.; Kociánová, M.; Hulík, J.; Plavčan, J.; Horňáčková, M.; Suchoňová, M.; Veis, P.; Cáceres, J.O. Discrimination of Copper Alloys with Archaeological Interest Using LIBS and Chemometric Methods. In Proceedings of the 2014 World Data System (WDS) Contributed Paper–Physics, Prague, Czech Republic, 3–5 June 2014; pp. 131–135.
37. Pořízka, P.; Klus, J.; Képeš, E.; Prochazka, D.; Hahn, D.W.; Kaiser, J. On the utilization of principal component analysis in laser-induced breakdown spectroscopy data analysis, a review. *Spectrochim. Acta Part B* **2018**, *148*, 65–82. [CrossRef]
38. Alexandrov, S.; Ivanov, G.; Hristova, T. The necropolis of Baley in Northwest Bulgaria and its significance for the end of the Bronze Age and the beginning of the Iron Age in the Lower Danube region. In *Southeast Europe and Anatolia in Prehistory: Essays in Honor of Vassil Nikolov on His 65th Anniversary*, 1st ed.; Bacvarov, K., Gleser, R., Eds.; Universitätsforschungen zur Prähistorischen Archäologie 293: Bonn, Germany, 2016; pp. 149–158.
39. Streli, C.; Wobrauschek, P.; Kregsamer, P. X-ray Fluorescence Spectroscopy, Applications. In *Encyclopedia of Spectroscopy & Spectrometry*; Lindon, J., Tranter, G., Holmes, J., Eds.; Academia Press Ltd.: Cambridge, MA, USA, 1999; pp. 2478–2487.
40. Towett, E.K.; Shepherd, K.D.; Cadisch, G. Quantification of total element concentrations in soils using total X-ray fluorescence spectroscopy (TXRF). *Sci. Total Environ.* **2013**, *463–464*, 374–388. [CrossRef]
41. Han, H.; Dang, S.; Acosta, J.C.; Fu, J.; Sondergeld, C.; Rai, C. X-ray Fluorescence and Laser-Induced Breakdown Spectroscopy for Advanced Rock Elemental Analysis. In Proceedings of the SPE/AAPG/SEG Unconventional Resources Technology Conference, Denver, CO, USA, 22–24 July 2019.
42. Erdem, A.; Çilingiroglu, A.; Giakoumaki, A.; Castanys, M.; Kartsonaki, E.; Fotakis, C.; Anglos, D. Characterization of Iron age pottery from eastern Turkey bylaser-induced breakdown spectroscopy (LIBS). *J. Archaeol. Sci.* **2008**, *35*, 2486–2494. [CrossRef]
43. Schröder, S.; Pavlov, S.G.; Rauschenbach, I.; Jessberger, E.K.; Hübers, H.W. Detection and identification of salts and frozen salt solutions combining laser-induced breakdown spectroscopy and multivariate analysis methods: A study for future martian exploration. *Icarus* **2013**, *223*, 61–73. [CrossRef]
44. Smith, L.A. *A Tutorial on Principal Components Analysis*; Computer Science Technical Report OUCS-2002-12; University of Otago: Dunedin, New Zealand, 2002.
45. Robbiola, R.; Blengino, J.M.; Fiaud, C. Morphology and mechanisms of formation of natural patinas on archaeological Cu-Sn alloys. *Corros. Sci.* **1998**, *40*, 2083–2111. [CrossRef]
46. National Institute of Standard and Technology. Available online: http://physics.nist.gov/PhysRefData/ASD/index.html (accessed on 27 April 2023).
47. Scott, D.A. *Metallography and Microstructure of Ancient and Historic Metals*; Getty Conservation Institute in Association with Archetype Books: Marina del Rey, CA, USA, 1991.
48. Papadimitriou, G. The technological evolution of copper alloys in the Aegean during the prehistoric period. In *Aegean Metallurgyin the Bronze Age*; Tzachili, I., Ed.; Ta Pragmata Publications: Athens, Greece, 2008; pp. 271–280.
49. Johannsen, J.W. Heavy Metal–lead in Bronze Age Scandinavia. *J. Swed. Antiqu. Res.* **2016**, *111*, 153–161.
50. Hurcombe, L.M. *Archaeological Artifacts as Material Culture*; Routledge: London, UK; New York, NY, USA, 2007.
51. Radivojević, M.; Roberts, B.W. Early Balkan Metallurgy: Origins, Evolution and Society, 6200–3700 BC. *J. World Prehist.* **2021**, *34*, 195–278. [CrossRef]
52. Otto, H.; Witter, W. *Handbuch der Ältesten Vorgeschichtlichen Metallurgie in Mitteleuropa*; Leipzig: Barth, Germany, 1957.